Fig. 5 for the weak shock solution. The relative error of the strong shock approximation are even smaller.

Conclusion

Approximate relations for both weak and strong oblique shock angles have been shown to be accurate for moderate to high supersonic Mach numbers and for wedge angles that are less than the maximum wedge angle.

References

[1]Dou, H. S., and Teng, H.-Y., "Approximate Formula of Weak Oblique Shock Wave Angle," *AIAA Journal*, Vol. 30, No. 3, 1992, pp. 837–839.

[2]Powers, J. M., "Comment on 'Approximate Formula of Weak Oblique Shock Wave Angle,'" *AIAA Journal*, Vol. 30, No. 11, 1992, pp. 2801, 2802.

[3]Anon., "Equations, Tables and Charts for Compressible Flow," Ames Aeronautical Lab., TR 1135, Moffett Field, CA, 1953

[4]Mascitti, V. R., "A Closed-form Solution to Oblique Shock-Wave Properties," *Journal of Aircraft*, Vol. 6, No. 1, 1969, p. 66.

[5]Liepman, H. W., and Roshko, A., *Elements of Gas Dynamics*, Wiley, New York, 1957, pp. 84–93.

Adaptive Computations of Flow Around a Delta Wing with Vortex Breakdown

David L. Modiano* and Earll M. Murman†
Massachusetts Institute of Technology, Cambridge, Massachusetts 02139

I. Introduction

THE next generation of fighter aircraft is being designed to fly at very high angle of attack, at which vortex breakdown occurs.[1] The two typical types of breakdown are the "bubble" form and the "spiral" form, which are characterized by the geometry of the flow downstream of the breakdown. This Note presents simulations of vortex breakdown above a stationary delta wing over a range of angles of attack. Adaptive refinement is used to add mesh nodes in the region of the vortex. Numerical simulations of vortex breakdown over a stationary delta wing have been reported by various researchers. No calculations have been reported using adaptive mesh methods.

II. Solution Method

Full details can be found in Ref. 2. The governing equations are the Euler equations for inviscid, compressible flow. The spatial discretization is a node-based trilinear Galerkin finite element method. Tetrahedral cell meshes are generated by the advancing wave front method of Peraire et al.[3] A mix of second- and fourth-difference artificial dissipation is added to insure stability. The fourth difference is constructed so that it vanishes when applied to a linear function, using the method of Holmes and Connell.[4] Temporal integration is performed by the four-stage method of Jameson et al.,[5] based on the Runge-Kutta method. The artificial dissipation is frozen after the second stage. Local time steps are used for steady flow solutions, based on an energy stability analysis by Giles.[6]

Received May 4, 1993; presented as Paper 93-3400 at the AIAA 11th Applied Aerodynamics Conference, Monterey, CA, Aug. 9–11, 1993; revision received Oct. 21, 1993; accepted for publication Oct. 21, 1993.

*Research Assistant, Computational Aerospace Sciences Laboratory, Deptartment of Aeronautics and Astronautics; currently Senior Research Associate, ICOMP, NASA Lewis Research Center, Cleveland, OH 44135. Member AIAA.

†Professor and Head, Deptartment of Aeronautics and Astronautics. Fellow AIAA.

III. Adaptation Procedure

Adaptive mesh-point embedding is used to increase the mesh resolution in the vicinity of interesting flow features. The adaptation procedure is as follows. The adaptation parameter is calculated at the mesh nodes. The nodes are marked for adaptation where the adaptation parameter exceeds a threshold. A mesh cell is subdivided into 12, 4, or 2 smaller cells, depending on how many of its corners are marked.

The entropy and the total pressure loss are attractive adaptation parameters for vortex flows, since they vanish in the irrotational limit. Both have been used successfully as adaptation parameters for delta wing flows.[7,8] In the present work the entropy was chosen, with the adaptation threshold set so that 30% of the coarse mesh nodes would be marked for refinement. This fraction was chosen so that the entire vortex is included in the adapted region, and it results in a quadrupling of the number of nodes and cells of the mesh.

IV. Stationary Wing Solutions

Stationary wing solutions were obtained at eight values of angle of attack, in the range of 0 to 42 deg. The angles of attack are concentrated in the high part of the range, in which vortex breakdown occurs. The leading-edge sweep back angle Λ is 75 deg, so the aspect ratio is 1.07. The freestream Mach number $M_\infty = 0.3$ for all cases. The geometry and Mach number were chosen to match those used by Ekaterinaris and Schiff[9] for their solutions.

The coarse mesh used for all cases has 15,462 nodes. The adapted meshes vary from 77,630 to 83,286 nodes.

A. Analysis of Global Features of Solutions

Stationary wing normal force curves are presented in Fig. 1, compared with Jarrah's wind tunnel-data.[10] Where two symbols are shown for the same angle of attack, the solution does not converge, which for the cases involving vortex breakdown is due to the inherent unsteadiness of the flow downstream of breakdown. The normal force coefficient is adequately predicted using the coarse mesh at low angles of attack, in which the vortex is intact over the entire wing. However, the coarse mesh is insufficient to

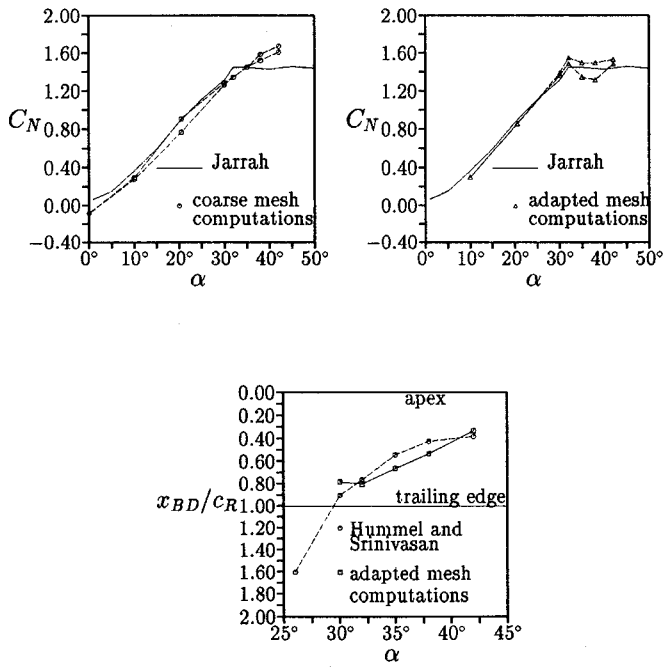

Fig. 1 Normal force coefficient and breakdown position vs angle of attack.

capture the details of breakdown well enough to predict the behavior at higher incidence. At all angles of attack, the adaptively computed coefficient of normal force is in good agreement with the wind-tunnel data.

The variation of vortex breakdown position with angle of attack is shown in Fig. 1, with experimental data of Hummel and Srinivasan.[11] The numerical breakdown position is defined as where the velocity in the direction of the axis of the intact vortex first becomes negative.

Reasonable agreement is seen between the computational and experimental breakdown position. The numerical breakdown position tends to be 5–10% of root chord aft of the experimental measurement. Two factors contribute to this difference. First, it may be due to a different criterion used to define breakdown position. The rapid expansion of the vortex core, which is easily identifiable in the wind tunnel by smoke visualization, occurs upstream of the onset of reversed flow, which is easily identifiable numerically by examination of the axial velocity. Thus, the numerical determination of the vortex breakdown position will be slightly aft of the experimental determination. The magnitude of this difference is estimated in Sec. IV.B.

Another source of the difference is the fluctuation of breakdown position due to the inherent unsteadiness of the flow. Fluctuation is present in the numerical solution, having a typical amplitude of 3% of root chord. Experimental measurements of breakdown position represent a time average of the unsteady breakdown position, whereas the numerical breakdown position is the instantaneous position at the iteration at which postprocessing is performed.

B. Vortex Breakdown at 32-deg Angle of Attack

Vortex breakdown occurs far aft above the wing. The solution is compared with that of Ekaterinaris and Schiff,[9] who solved the Navier-Stokes equations with a structured grid of about 100,000 grid points outside the boundary layer. The jagged appearance of the contour plots is due to the interpolation of the solution on an irregular mesh in postprocessing, and is a consequence of the large second derivative of the solution.

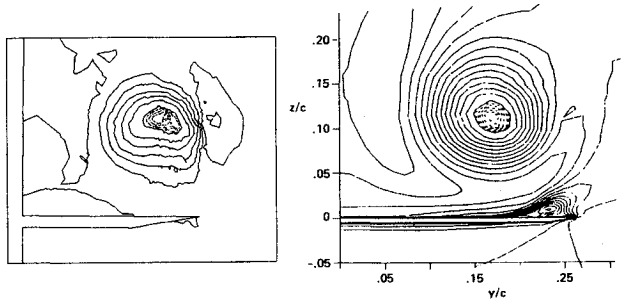

Fig. 2 Axial velocity $x/c_R = 0.90$, for $\alpha = 32$ deg. Left: present adapted mesh; right: from Ref. 9. Solid lines are positive values; contour increment is 0.05. Dashed lines are negative values; contour increment is 0.01.

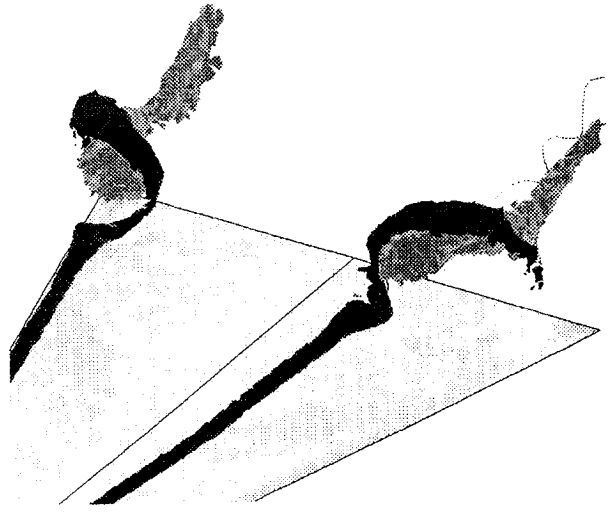

Fig. 3 Vortex breakdown region, showing the vortex core and the region of reversed flow for $\alpha = 32$ deg, on adapted mesh.

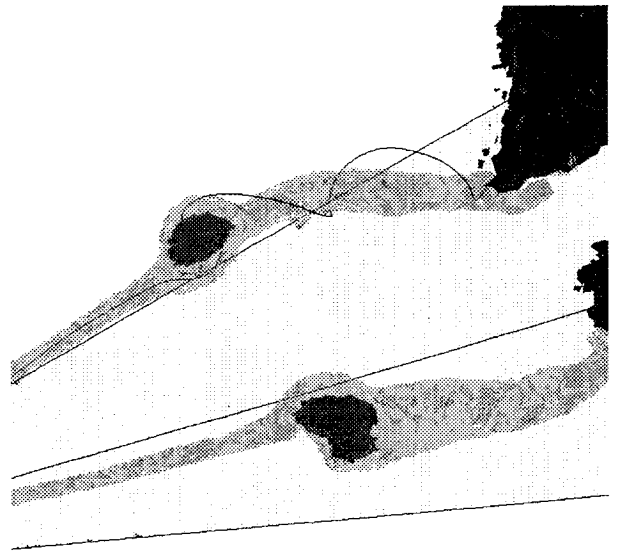

Fig. 4 Vortex breakdown region, showing the vortex core and the region of reversed flow for $\alpha = 42$ deg, on adapted mesh.

Figure 2 shows the axial velocity in a plane normal to the wing at 90% of root chord, as computed on the present adapted mesh, and as presented in Ref. 9. Both solutions show a small region of reversed flow at the vortex axis, which indicates the presence of vortex breakdown. The symmetric shape of the reversed flow region in Ref. 9 indicates the "bubble" type of breakdown, an assertion which is supported by particle traces in the region of breakdown, and by the lack of unsteadiness in the solution.

The present solution shows significant unsteadiness, and visualization reveals the breakdown to be of the spiral type. The unsteadiness in the present work is due to the rotation of the spiral vortex about the original vortex axis. Figure 3 shows the breakdown region. The vortex core, represented as the region of high entropy, follows a spiral path around the region of reversed flow, with the opposite sense of rotation from the flow in the vortex.

In swirling pipe flow, breakdown can sometimes manifest in either the spiral or the bubble form at identical flow conditions.[12] A possible explanation for the difference in type of breakdown seen in the two numerical solutions is that the flow conditions are among those at which both types of breakdown are possible, with the choice determined by properties of the two solvers. For example, the structured grid of Ref. 9 might more readily support an axisymmetric form of breakdown than it would the spiral form, since one set of grid lines lies along rays through the apex of the wing. The spiral type of breakdown is more commonly observed in delta wing flows than is the bubble type, possibly due to an instability of the bubble form.[1]

Figure 3 also illustrates the different criteria for the vortex breakdown position which were mentioned in Sec. IV.A. Two criteria which can be measured experimentally are the location at which the vortex core begins to expand, and the location at which the core leaves the axis. These are 10% and 5% of root chord forward of the onset of reversed flow, respectively. This is in accord with the differences between the numerical and experimental breakdown positions seen in Fig. 1.

C. Vortex Breakdown at 42-deg Angle of Attack

In this flow, bubble type breakdown occurs at 33% of root chord, followed by reformation of a coherent vortex, and spiral breakdown further downstream. Figure 4 shows the region near breakdown. The bubble extends 4% of root chord downstream,

being followed by a thicker but coherent vortex that attains 70% of the freestream axial velocity at its center before it spirals away from the axis and begins to dissipate. The helical vortex spirals around a large region of reversed flow which begins at 55% of root chord and extends downstream of the trailing edge of the wing.

The reformation of the vortex downstream of breakdown, although not typical of delta wing flows, has been noted in experiments and calculations of breakdown in swirling pipe flows.[12,13] The coarse mesh solution shows no indication of the bubble breakdown, which suggests that further differences could appear with additional refinement.

V. Conclusion

An adaptive mesh Euler solver was used to simulate the flow over a sharp edged delta wing. Adaptation enables the normal force to be well predicted at high range of angle of attack in the prescence of vortex breakdown. The position of breakdown is in reasonable agreement with experimental measurements. Vortex breakdown is predicted to primarily exhibit the spiral form, which is typically observed in delta wing experiments.

Acknowledgments

This work was supported by Air Force Office of Scientific Research Contract AFOSR-89-0395A, monitored by L. Sakell; and by the McDonnell Aircraft Company under MDC/MDRL IRAD Sponsorship. The authors would like to thank Jaime Peraire of Massachusetts Institute of Technology, Ken Morgan of University College, Swansea, Wales, and Joaquin Peiró of the Imperial College of Science, Technology, and Medicine, London, England, for the use of the mesh generation system.

References

[1]Lambourne, N. C., and Bryer, D. W., "The Bursting of Leading-Edge Vortices—Some Observations and Discussions of the Phenomenon," Aeronautical Research Council, R & M 3283, 1961.

[2]Modiano, D. L., "Adaptive Mesh Euler Equation Computation of Vortex Breakdown in Delta Wing Flow," Ph.D. Thesis, Massachusetts Inst. of Technology, Cambridge, MA, Feb. 1993; also Massachusetts Inst. of Technology Computational Aerospace Sciences Lab. Rept. CASL-TR-93-001, Cambridge, MA, Jan. 1993.

[3]Peraire, J., Morgan, K., and Peiró, J., "Unstructured Finite Element Mesh Generation and Adaptive Procedures for CFD," *Application of Mesh Generation to Complex 3-D Geometries*, AGARD-CP-464, May 1989.

[4]Holmes, D. G., and Connell, S. D., "Solution of the 2D Navier-Stokes Equations on Unstructured Adaptive Grids," AIAA Paper 89-1932, June 1989.

[5]Jameson, A., Schmidt, W., and Turkel, E., "Numerical Solutions of the Euler Equations by Finite Volume Methods Using Runge-Kutta Time-Stepping Schemes," AIAA Paper 81-1259, June 1981.

[6]Giles, M. B., "Energy Stability Analysis of Multi-Step Methods on Unstructured Meshes," Massachusetts Inst. of Technology Computational Fluid Dynamics Lab. Rept. CFDL-TR-87-1, Cambridge, MA, March 1987.

[7]Borsi, M., Formaggia, L., Hettena, E., Santillan, S., Selmin, V., and Tarditi, S., "Vortical Flow Simulation by Using Structured and Unstructured Grids," *Vortex Flow Aerodynamics*, AGARD-CP-494, Oct. 1990.

[8]Melton, J. E., Thomas, S. D., and Cappucio, G., "Unstructured Euler-Flow Solutions Using Hexahedral Cell Refinement," AIAA Paper 91-0637, Jan. 1991.

[9]Ekaterinaris, J. A., and Schiff, L. B., "Vortical Flows Over Delta Wings and Numerical Prediction of Vortex Breakdown," AIAA Paper 90-0102, Jan. 1990.

[10]Jarrah, M. A., "Unsteady Aerodynamics of Delta Wings Performing Maneuvers to High Angle of Attack," Ph.D. Thesis, Stanford Univ., Stanford, CA, Dec. 1988.

[11]Hummel, D., and Srinivasan, P. S., "Vortex Breakdown Effects on the Low-Speed Aerodynamic Characteristics of Slender Delta Wings in Symmetrical Flow," *Royal Aeronautical Society Journal*, Vol. 71, April 1967, pp. 319–322.

[12]Sarpkaya, T., "On Stationary and Travelling Vortex Breakdowns," *Journal of Fluid Mechanics*, Vol. 45, Feb. 1971, pp. 545–559.

[13]Lopez, J. M., "Axisymmetric Vortex Breakdown, Part 1. Confined Swirling Flow," *Journal of Fluid Mechanics*, Vol. 221, Dec. 1990, pp. 533–552.

Numerical Computations of Supersonic Base Flow with Special Emphasis on Turbulence Modeling

Jubaraj Sahu*
U.S. Army Research Laboratory,
Aberdeen Proving Ground, Maryland 21005

Introduction

ONE of the important parameters in the design of shells is the total aerodynamic drag. The base drag component is a large part and can be as high as 50% or more of the total drag. Therefore, it is necessary to predict the base pressure as accurately as possible. The ability to compute the base region flowfield for projectiles using Navier-Stokes computational techniques has been developed.[1] This capability is very important for determining aerodynamic coefficient data including the total aerodynamic drag. A number of base flow calculations have been made, and base drag and total drag have been predicted with reasonable accuracy. However, due to the lack of available data, the base flow predictive capabilities have not been assessed with detailed base pressure distribution, mean flow velocity components, and turbulence quantities. This is especially true of the base flow for axisymmetric bodies at transonic and supersonic speeds. Recently, experimental measurements[2] have been made in the base region for supersonic flow over a cylindrical afterbody. The data includes base pressure distribution (over the base), mean flow, as well as turbulence quantities.

Figure 1 is a schematic diagram showing the important features of supersonic base flow. The approaching supersonic turbulent boundary layer separates at the base corner, and the free shear layer region is formed in the wake. The flow expands at the base corner and is followed by the recompression shock downstream of the base which realigns the flow. The flow then redevelops in the trailing wake. A low-pressure region is formed immediately downstream of the base which is characterized by a low-speed recirculating flow region. Interaction between this recirculating region and the inviscid external flow occurs through the free shear mixing region. This is the region where turbulence plays an important role. The basic configuration used in this study is a cylindrical afterbody. Numerical flowfield computations have been performed at $M_\infty = 2.46$ and at 0-deg angle of attack. Various turbulence models (two algebraic models and a two-equation model) are used in the base flow region. Details of the flowfield such as Mach number contours and base pressure distributions are presented. Computed base pressure distributions are compared with available experimental data for the same conditions and the same configuration.

Turbulence Models

The complete set of time-dependent, Reynolds-averaged, thin-layer Navier-Stokes equations is solved numerically using an implicit finite-difference scheme. For turbulent base flow calculations, two algebraic models (Baldwin and Lomax[3] and Chow[4]) and a two-equation k-ε eddy viscosity turbulence model have been used.

Baldwin-Lomax Model

This is a two-layer model in which an eddy viscosity is calculated for an inner and an outer region. The inner region follows the Prandtl-Van Driest formulation. In both the inner and outer formulations, the distribution of vorticity is used to determine the length scales, thereby avoiding the necessity of finding the outer edge of the boundary layer.

Presented as Paper 92-4352 at the AIAA Atmospheric Flight Mechanics Conference, Hilton Head, SC, Aug. 10–12, 1992; received May 12, 1993; revision received Jan. 2, 1994; accepted for publication Jan. 3, 1994.

*Aerospace Engineer. Associate Fellow AIAA.